An adaptive Fuzzy C-means method utilizing neighboring information for breast tumor segmentation in ultrasound images

Yuan Feng[a)]
Center for Molecular Imaging and Nuclear Medicine, School of Radiological and Interdisciplinary Sciences (RAD-X), Soochow University, Collaborative Innovation Center of Radiation Medicine of Jiangsu Higher Education Institutions, Suzhou, Jiangsu 215123, China
School of Mechanical and Electronic Engineering, Soochow University, Suzhou, Jiangsu 215021, China
School of Computer Science and Engineering, Soochow University, Suzhou, Jiangsu 215021, China

Fenglin Dong
Department of Ultrasounds, the First Affiliated Hospital of Soochow University, 188 Shizi Street, Suzhou 215006, China

Xiaolong Xia
Center for Molecular Imaging and Nuclear Medicine, School of Radiological and Interdisciplinary Sciences (RAD-X), Soochow University, Collaborative Innovation Center of Radiation Medicine of Jiangsu Higher Education Institutions, Suzhou, Jiangsu 215123, China

Chun-Hong Hu
Department of Radiology, the First Affiliated Hospital of Soochow University, 188 Shizi Street, Suzhou 215006, China

Qianmin Fan
Department of Ultrasounds, the First Affiliated Hospital of Soochow University, 188 Shizi Street, Suzhou 215006, China

Yanle Hu
Department of Radiation Oncology, Mayo Clinic in Arizona, Phoenix, AZ, USA

Mingyuan Gao
Center for Molecular Imaging and Nuclear Medicine, School of Radiological and Interdisciplinary Sciences (RAD-X), Soochow University, Collaborative Innovation Center of Radiation Medicine of Jiangsu Higher Education Institutions, Suzhou, Jiangsu 215123, China

Sasa Mutic
Department of Radiation Oncology, Washington University, St. Louis, MO, USA

(Received 23 November 2016; revised 24 April 2017; accepted for publication 10 May 2017; published 16 June 2017)

Purpose: Ultrasound (US) imaging has been widely used in breast tumor diagnosis and treatment intervention. Automatic delineation of the tumor is a crucial first step, especially for the computer-aided diagnosis (CAD) and US-guided breast procedure. However, the intrinsic properties of US images such as low contrast and blurry boundaries pose challenges to the automatic segmentation of the breast tumor. Therefore, the purpose of this study is to propose a segmentation algorithm that can contour the breast tumor in US images.

Methods: To utilize the neighbor information of each pixel, a Hausdorff distance based fuzzy c-means (FCM) method was adopted. The size of the neighbor region was adaptively updated by comparing the mutual information between them. The objective function of the clustering process was updated by a combination of Euclid distance and the adaptively calculated Hausdorff distance. Segmentation results were evaluated by comparing with three experts' manual segmentations. The results were also compared with a kernel-induced distance based FCM with spatial constraints, the method without adaptive region selection, and conventional FCM.

Results: Results from segmenting 30 patient images showed the adaptive method had a value of sensitivity, specificity, Jaccard similarity, and Dice coefficient of $93.60 \pm 5.33\%$, $97.83 \pm 2.17\%$, $86.38 \pm 5.80\%$, and $92.58 \pm 3.68\%$, respectively. The region-based metrics of average symmetric surface distance (ASSD), root mean square symmetric distance (RMSD), and maximum symmetric surface distance (MSSD) were 0.03 ± 0.04 mm, 0.04 ± 0.03 mm, and 1.18 ± 1.01 mm, respectively. All the metrics except sensitivity were better than that of the non-adaptive algorithm and the conventional FCM. Only three region-based metrics were better than that of the kernel-induced distance based FCM with spatial constraints.

Conclusion: Inclusion of the pixel neighbor information adaptively in segmenting US images improved the segmentation performance. The results demonstrate the potential application of the method in breast tumor CAD and other US-guided procedures.
[https://doi.org/10.1002/mp.12350]

Key words: adaptive selection, breast tumor, FCM, image segmentation, ultrasound imaging

1. INTRODUCTION

Breast cancer is one of the leading types of cancers in new cancer cases in females, and the leading cause of cancer deaths in both economically developing and developed countries. A total of 1,383,500 newly diagnosed breast cancer cases was reported worldwide in 2008.[1] Early detection using biomedical imaging techniques is crucial for breast cancer treatment, for example, X-ray mammography[2] and ultrasound (US) imaging.[3] Although X-ray mammography is a common practice, US has been shown to aid detection of small mammographically occult breast cancers and increase the overall cancer detection rate.[4–6] Therefore, the computer-aided diagnosis (CAD) based on ultrasound images has become an emerging approach for improving the diagnostic efficiency and accuracy.[7,8] In CAD, delineation of the breast tumor is a crucial step for breast cancer screening and diagnosis. Manual segmentation and inspection of the breast tumor require extensive training for the observers and the inter-observer difference could be large. Besides CAD, automatic detection and selection of the tumor lesion is also crucial for interventional procedures such as imaged-guided biopsy.[9] Therefore, an automatic image segmentation method is important to increase the quality, reproducibility, and efficiency of the breast tumor diagnosis, and to improve the US-guided procedures.

US images have intrinsic properties such as speckle noise, low contrast, and blurred boundaries, which pose challenges for image segmentation.[10,11] Many methods have been proposed to overcome these problems,[12–16] especially for segmenting US images of breast tumors. Gu et al. (2016) applied a watershed method to delineate the tumor boundary before region classification in CAD. Huang et al. (2015) used a graph-based segmentation to segment different regions. The tumor region was then selected and refined by an active contour method. Guo et al. (2016) segmented the tumor region using a level-set method based on the calculation of the neutrosophic similarity score (NSS). Among these segmentation techniques, region recognition and selection are needed for the watershed and graph-based methods, and initial contours are needed for the level-set method. Although satisfactory results could be achieved, a method with minimal processing steps and robust to noise is still required for effective segmentation of the tumor.

As an unsupervised method, the fuzzy c-means (FCM) method is robust to noise and does not require initial contours and prior information.[17,18] Therefore, FCM has been widely used to segment US images[19,20] and images with blurred boundaries.[21,22] Many modifications and improvements of the FCM method have been proposed, for example, relational FCM,[23] spatial models,[24] probability based FCM,[25,26] and a neutrosophic c-means (NCM) clustering algorithm.[16] It has been revealed that different distance measure based FCM can increase the performance and robustness of the classical FCM algorithm.[27–31] Notably, Chen and Zhang (2004) are among the first to introduce a kernel-induced distance measure to FCM and showed the algorithm was robust to noise. However, most of the FCM based segmentation focused on MR images, and an improved FCM method is still needed for segmenting US images.

In this study, we combined a Hausdorff-based FCM algorithm with an adaptive region selection scheme for segmenting the US images of breast tumor. Based on mutual information of the regions, the neighbor region surrounding each pixel was selected adaptively for the Hausdorff distance measurement. Results demonstrated that the adaptive Hausdorff-based FCM algorithm had a better performance than the Hausdorff-based and traditional FCM algorithms. Automated segmentation of breast tumors can potentially help US image-based breast cancer diagnosis, intervention, and treatment.

2. MATERIALS AND METHODS

2.A. Euclid and Hausdorff distance based FCM

In standard FCM, each image pixel $x_i (i = 1 \ldots n)$ was clustered into c groups by minimizing an objective function

$$J = \sum_{i=1}^{n} \sum_{k=1}^{c} u_{ik}^{m} \|x_i - v_k\|^2, \tag{1}$$

where $v_k (k = 1 \ldots c)$ are the cluster centroids, membership function u_{ik} satisfies $\sum_{k=1}^{c} u_{ik} = 1, \forall i \ (0 \le u_{ik} \le 1, \forall i, k)$, and m is the value controlling the fuzziness of segmentation. Conventionally, the distance between each gray-level pixel-valued scalar x_i and the centroid value scalar v_k is defined by Euclid distance. In a previous study, we found that a Hausdorff distance based FCM (HFCM) is useful to segment MR images.[29] In HFCM, Euclid distance was replaced with Hausdorff distance:

$$\|p_i - p_j\|_H = \max\left\{ \sup_{p_i \in A} \inf_{p_j \in B} |p_j - p_i|, \sup_{p_j \in B} \inf_{p_i \in A} |p_i - p_j| \right\}, \tag{2}$$

where $A = \{p_i | p_i \in A\}$ and $B = \{p_j | p_j \in B\}$ are two non-empty pixel subsets with pixel p_i or p_j located at the center [Fig. 1(a)]. Correspondingly, the objective function and membership functions were

$$J_H = J + \alpha \sum_{i=1}^{n} \sum_{k=1}^{c} u_{ik}^{m} \|x_i - v_k\|_H^2 \quad \text{and}$$
$$u_{ik} = \frac{\left(\|x_i - v_k\|^2 + \alpha \|x_i - v_k\|_H^2 \right)^{\frac{1}{m-1}}}{\sum_{l=1}^{c} \left(\|x_i - v_l\|^2 + \alpha \|x_i - v_l\|_H^2 \right)^{\frac{1}{m-1}}}, \tag{3}$$

where α is the weighting ratio. We took $m = 2$ and $c = 3$ for the comparative analysis with other FCM based algorithms in this study.

2.B. Adaptive region selection for HFCM (AHFCM)

The image contrast of US images are relatively low compared with imaging modalities such as conventional MR, especially at the target boundaries. Therefore, we propose to

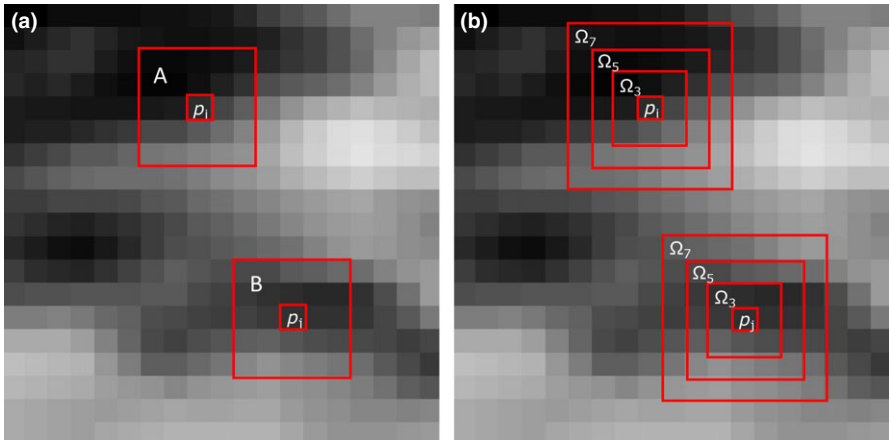

FIG. 1. (a) Hausdorff distance between the two pixel regions A and B. The distance is measured between the pixels p_i and p_j in each region, (b) Three neighbor regions Ω_3, Ω_5, and Ω_7 enclosing pixels p_i and p_j, each has a size of 3 × 3, 5 × 5, and 7 × 7 pixels, respectively. [Color figure can be viewed at wileyonlinelibrary.com]

select the neighboring region adaptively with respect to each pixel, as defined in Eq. (2). If the mutual information of two regions of pixels $A = \{p_i | p_i \in A\}$ and $B = \{p_j | p_j \in B\}$ [Fig. 1(a)] is $I(A, B)$, the size of A and B can be determined by comparing $I_3(A_{\Omega_3}, B_{\Omega_3})$, $I_5(A_{\Omega_5}, B_{\Omega_5})$, and $I_7(A_{\Omega_7}, B_{\Omega_7})$. In the above notation, p_i and p_j is located at the center with a neighbor region sizes of 3 × 3, 5 × 5, and 7 × 7 pixels, denoted by Ω_3, Ω_5., and Ω_7 [Fig. 1(b)]. Therefore, Eq. (2) is modified by:

$$\|p_i - p_j\|_{H_{\Omega_r}} = \max\left\{ \sup_{p_i \in A_{\Omega_r}} \inf_{p_j \in B_{\Omega_r}} |p_j - p_i|, \sup_{p_j \in B_{\Omega_r}} \inf_{p_i \in A_{\Omega_r}} |p_i - p_j| \right\} \tag{4}$$

with

$$r = \sup_{s \in \{3,5,7\}} \{I_s(A_{\Omega_s}, B_{\Omega_s})\} \tag{5}$$

where Ω_s (s = 3,5,7) is the three neighbor regions, and I_s is the mutual information.

By integrating this adaptive neighbor region selection scheme into the Hausdorff-based FCM method, the objective and membership functions are

$$J_{H_{\Omega_r}} = J + \alpha \sum_{i=1}^{n} \sum_{k=1}^{c} u_{ik}^m \|x_i - v_k\|_{H_{\Omega_r}}^2, \text{ and}$$
$$u_{ik} = \frac{\left(\|x_i - v_k\|^2 + \alpha \|x_i - v_k\|_{H_{\Omega_r}}^2\right)^{-\frac{1}{m-1}}}{\sum_{l=1}^{c} \left(\|x_i - v_l\|^2 + \alpha \|x_i - v_l\|_{H_{\Omega_r}}^2\right)^{-\frac{1}{m-1}}}, \tag{6}$$

where α is the weighting ratio, and r is determined by Eq. (6). For initialization of the centroid values v_k, we used the equally distributed values between the maximum and minimum pixel values of the image. The membership function were iteratively updated by Eq. (6) and the centroid values were updated by $v_k = \frac{\sum_{i=1}^{n} u_{ik}^m x_i}{\sum_{i=1}^{n} u_{ik}^m}$, until the objective function converges (Fig. 2). For the final contouring of the breast tumor, necessary morphological image processing steps were used for post-processing.[22]

2.C. Clinical images

Clinical breast cancer US images were acquired from the first affiliated hospital of Soochow University, with patient identity information removed. To acquire the tumor image, the depth focus ranged from 1 cm to 3 cm. A wide-band, high-frequency (4–13 MHz) linear-array transducer was used. A total of 30 Images were acquired from 30 different patients, respectively, with both malignant (n = 12) and benign (n = 18) breast cancer. All US images were produced by trained physicians using an Esaote 6100 model (Esaote, Genova, Italy) ultrasound imaging device. Original images were stored in DICOM format with 550 × 800 pixels that contains both the image and scanning information (Fig. 3). To evaluate and compare the performance of segmentation algorithms in contouring the tumor ROI, a reduced field of view (FOV) with 300 × 300 pixels containing the tumor was selected. A histogram equalization was applied to each image before segmentation.

2.D. Evaluation metrics

To evaluate the segmentation performance of the proposed method, we compared the automatically segmented contours with manual segmentations. To reduce the inter-observer difference, three physicians delineated the manual contours. The inter-observer differences were quantified by an inter-observer agreement index (IAI)[32]

$$IAI = 1 - \frac{|x_a - x_b|}{(x_a + x_b)/2} \tag{7}$$

where x_a and x_b are the numbers of the pixels within the regions contoured by the two different experts, respectively.

Both region-based and distance-based evaluation metrics were used to assess the algorithm. For region-based measure, sensitivity, specificity, Jaccard similarity, and Dice coefficient were used for the evaluation. These values test the region similarity from different perspectives. For distance-based measure, we used average symmetric surface distance

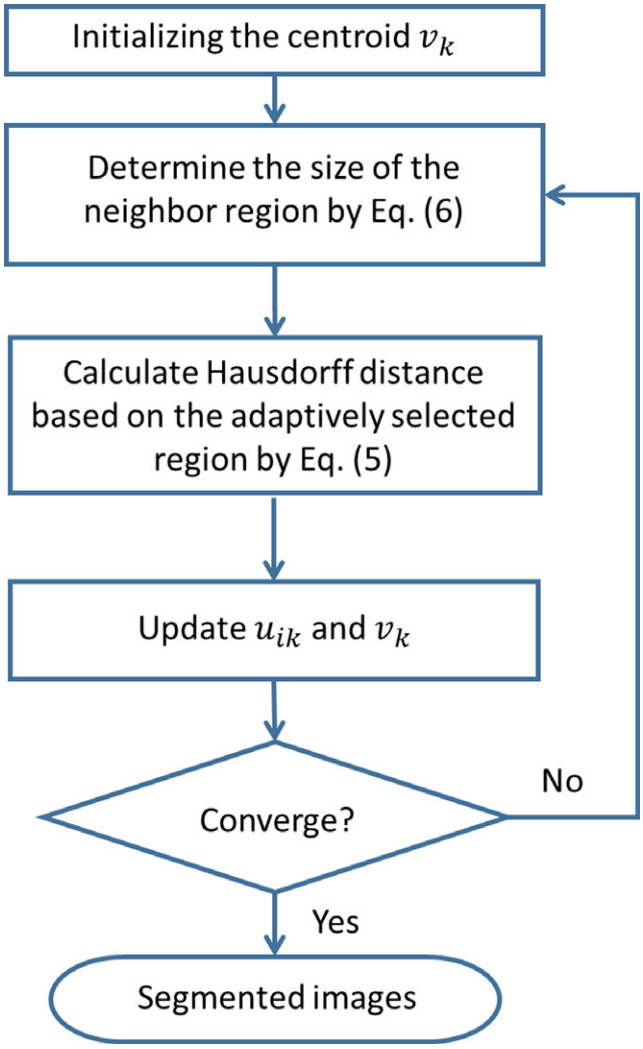

FIG. 2. A flow chart of the modified FCM algorithm based on the neighbor information. The size of the neighbor region is determined by adaptively comparing the mutual information value of the three regions Ω_3, Ω_5, and Ω_7. [Color figure can be viewed at wileyonlinelibrary.com]

(ASSD), root mean square symmetric distance (RMSD), maximum symmetric surface distance (MSSD) to evaluate the segmented region and the manual contours. By expressing the regional differences in terms of distances in space, these metrics evaluate the performance of the segmentation from another perspective. Details of these seven different metrics and its calculations were summarized in Appendix. We compared the performance of the AHFCM method with the HFCM and standard FCM method. In addition, we also compared the algorithms with the FCM with spatial constraints based on kernel-induced distance using mean filter (KFCM_S1), proposed by Chen and Zhang (2004). Two tailed, paired student *t*-tests (significance level of 5%) were used to compare the differences between these methods based on each metric.

3. RESULTS

Sample delineation of a benign [Figs. 4(a)– 4(c)] and malignant [Figs. 4(d)– 4(f)] breast tumor from the three experts showed a lower inter-observer variance for delineating the benign tumor (Fig. 5). The IAI value for expert 1 vs. 2, 1 vs. 3, and 2 vs. 3 were of 0.92 $\pm$ 0.06, 0.94 $\pm$ 0.06, and 0.93 $\pm$ 0.05 for benign tumors, respectively, contrasting to IAI values for malignant tumors, that is, 0.89 $\pm$ 0.15, 0.94 $\pm$ 0.08, and 0.90 $\pm$ 0.15.

Sample segmentation results are shown in Fig. 6. Using the evaluation metrics, we assessed the performance of the AHFCM by comparing the segmented images obtained by the three experts (Table I). For region-based evaluation metrics, all evaluation values were 80% higher, with a maximum mean value of 98.57% for specificity compared with the delineation of the expert 1. The minimum mean value of 83.87% is the Jaccard similarity when compared with the delineation of expert 2. A similar pattern was also observed for the distance-based evaluation metrics. The maximum mean value is 1.68 mm of MSSD when compared with the expert 2, while the minimum mean value is 0.01 of ASSD when compared with the expert 1.

To compare the segmentation performance of AHFCM with that of KFCM_S1, HFCM and FCM, we also calculated the evaluation metrics with these three methods, according to the manual contours of the three experts. For KFCM_S1, the maximum mean metric value of the region-based evaluation was 98.07% of specificity compared with the expert 3 (Table II). The minimum value was 81.23% of Jaccard

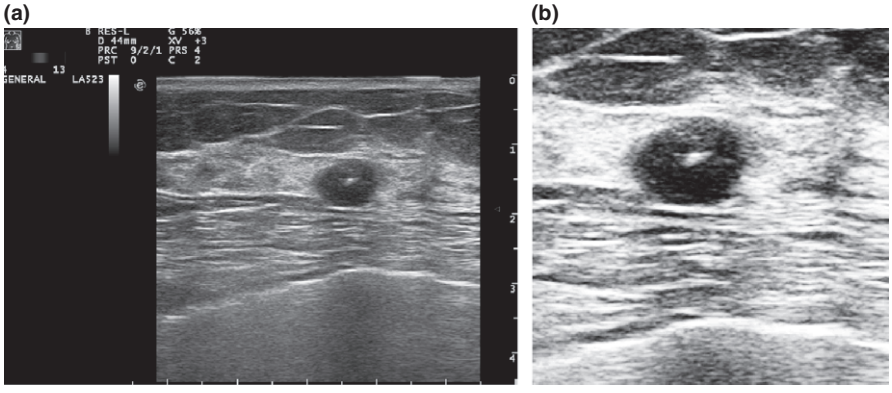

FIG. 3. (a) Original US images acquired with a resolution of 550 $\times$ 880, (b) Tumor ROI with 300 $\times$ 300 pixels with histogram equalization applied.

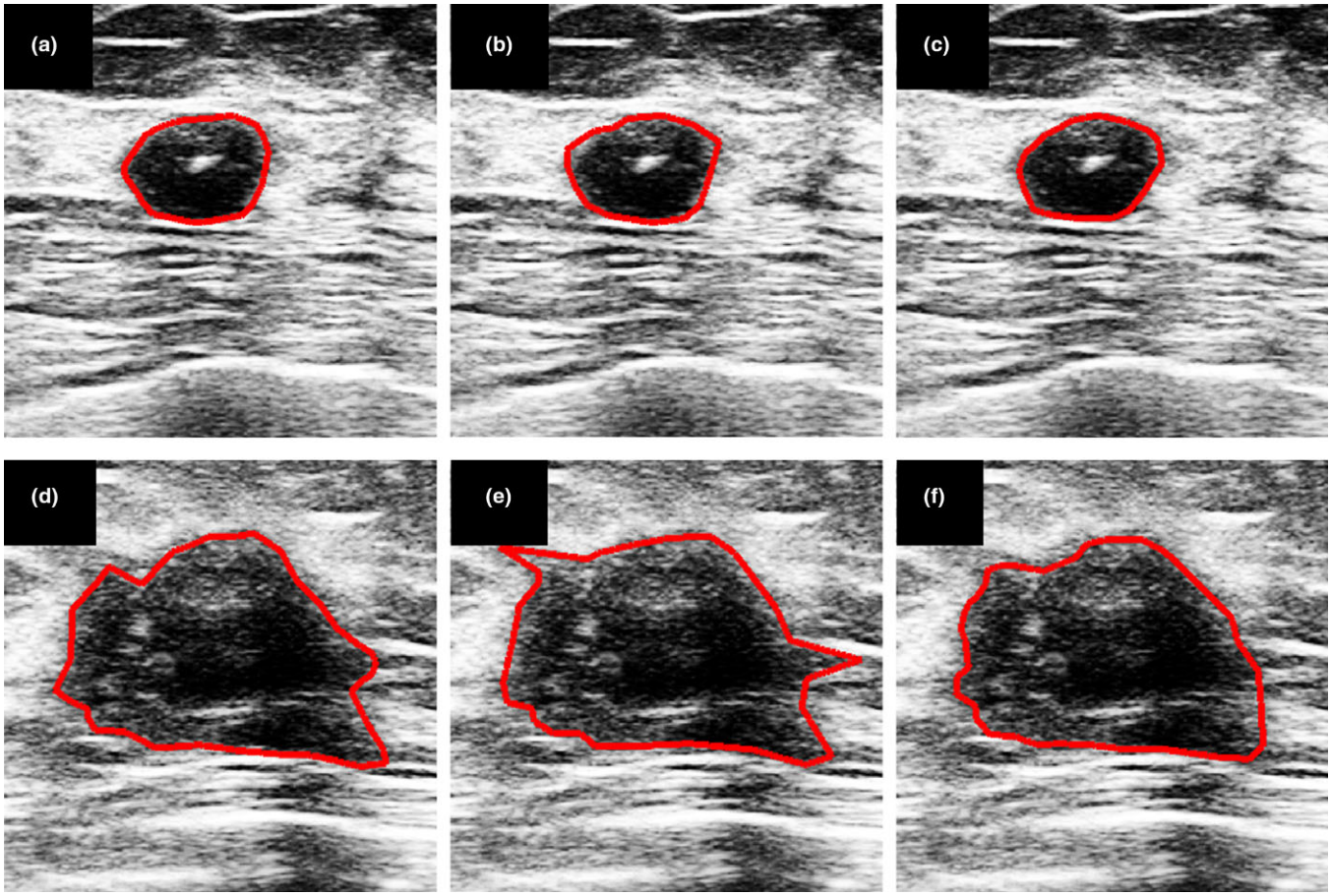

FIG. 4. Expert manual segmentation of the (a-c) benign and (d-f) malignant tumor with each contour being delineated by a radiologist. [Color figure can be viewed at wileyonlinelibrary.com]

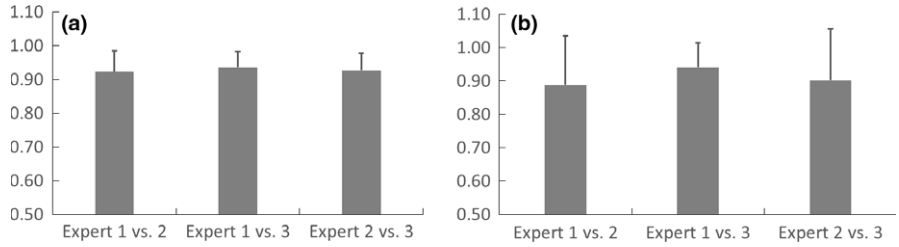

FIG. 5. The Inter-observer differences of the IAI values for contouring the (a) benign and (b) malignant tumors.

similarity compared with the expert 2. For distance-based evaluation, the maximum mean value was 2.14 mm of MSSD from both the expert 1 and 2, while the minimum mean value was 0.05 mm of both ASSD and RMSD from the expert 3.

For HFCM, the maximum mean metric value of the region-based evaluation was 97.43% of specificity compared with the expert 1 (Table III). The minimum value was 80.68% of Jaccard similarity compared with the expert 2. For distance-based evaluation, the maximum mean value was 2.34 mm of MSSD from the expert 3, while the minimum mean value was 0.06 mm of RMSD from the expert 1.

For the standard FCM (Table IV), the maximum mean value of the region-based evaluation metric is specificity compared with the expert 1 (97.43%). The minimum value is 79.52% of Jaccard similarity compared with the expert 2. The maximum distance evaluation metric is MSSD of 2.42 mm compared with the expert 3, while the minimum value is ASSD of 0.1 mm compared with the expert 1.

To assess the overall performance, we compared the three segmentation methods by combining the region-based evaluation metric values from the three experts, as shown in Fig. 7. A student *t*-test was used to quantify the differences between AHFCM and the other three methods. The corresponding p-values are summarized in Table V. Based on the region-based evaluation metrics, AHFCM exhibits significantly higher values of Jaccard similarity and Dice coefficient than

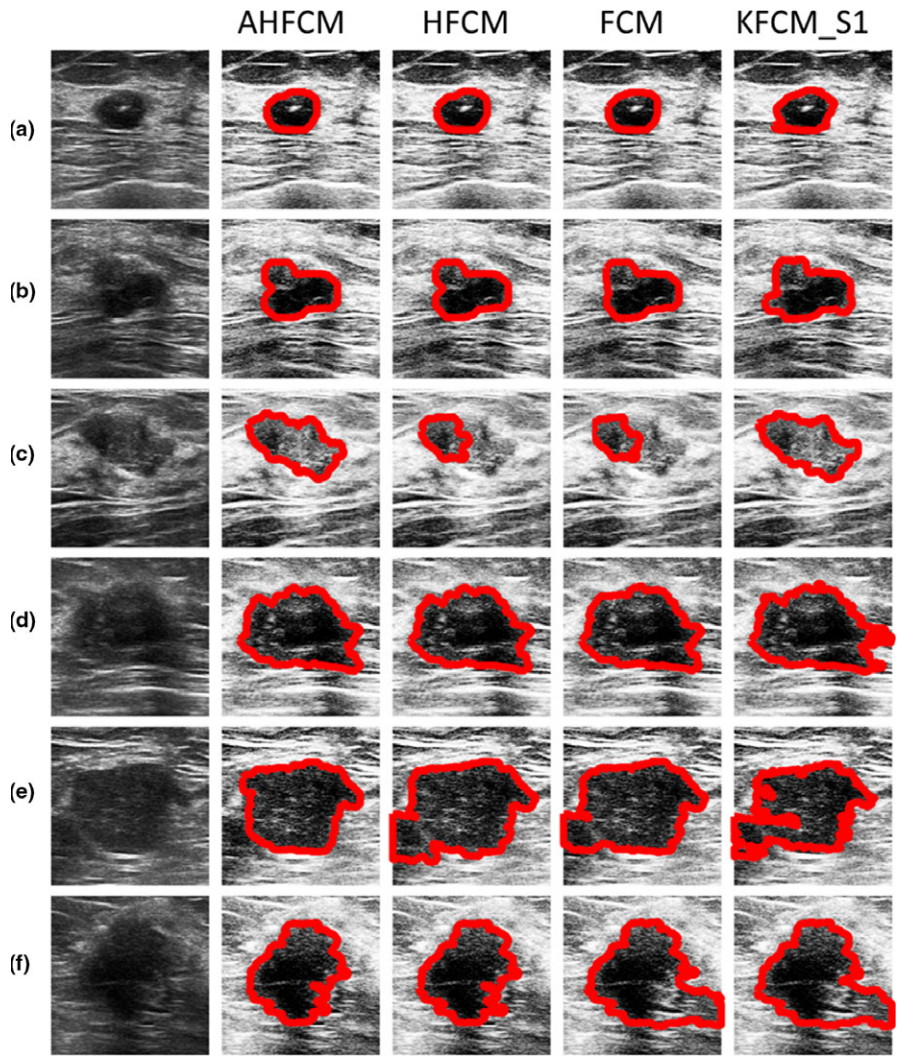

FIG. 6. A comparison of segmentation results for (a-c) benign and (d-f) malignant tumors from different algorithms. The first column from left are the original US images, while the segmented contours were drawn on images after histogram equalization. [Color figure can be viewed at wileyonlinelibrary.com]

TABLE I. Mean and standard deviation of the performance metric values of AHFCM obtained based on different expert contours.

	Expert 1	Expert 2	Expert 3
Sensitivity (%)	94.19 ± 1.90	92.21 ± 8.35	94.41 ± 3.30
Specificity (%)	98.57 ± 0.97	97.50 ± 2.51	97.42 ± 2.53
Jaccard (%)	88.96 ± 2.35	83.87 ± 7.95	86.30 ± 4.60
Dice (%)	94.14 ± 4.32	91.01 ± 5.23	92.58 ± 2.72
ASSD (mm)	0.01 ± 0.01	0.05 ± 0.06	0.03 ± 0.04
RMSD (mm)	0.03 ± 0.01	0.05 ± 0.03	0.05 ± 0.03
MSSD (mm)	1.11 ± 0.51	1.68 ± 1.13	1.65 ± 1.20

TABLE II. Mean and standard deviation of the performance metric values of KFCM_S1 obtained based on different expert contours.

	Expert 1	Expert 2	Expert 3
Sensitivity (%)	91.70 ± 5.47	89.58 ± 6.30	89.51 ± 7.20
Specificity (%)	97.70 ± 2.78	97.73 ± 2.37	98.07 ± 2.26
Jaccard (%)	83.57 ± 5.24	81.23 ± 7.69	82.38 ± 5.90
Dice (%)	90.96 ± 3.16	89.43 ± 5.06	90.23 ± 3.59
ASSD (mm)	0.06 ± 0.10	0.07 ± 0.13	0.05 ± 0.08
RMSD (mm)	0.06 ± 0.05	0.06 ± 0.05	0.05 ± 0.04
MSSD (mm)	2.14 ± 2.14	2.14 ± 2.18	1.87 ± 2.07

the other three methods. In addition, AHFCM had significantly higher specificity than HFCM and FCM, and higher sensitivity than KFCM_S1.

By comparing the three methods using the distance-based evaluation metrics, we found that AHFCM can give rise to significantly lower RMSD and MSSD than HFCM and FCM (Fig. 8). Although the mean values of ASSD, RMSD, and MSSD of AHFCM were lower than that of KFCM_S1, no significant differences were observed.

4. DISCUSSION

In this study, we present an adaptive region selection scheme for the Hausdorff distance based FCM to segment

TABLE III. Mean and standard deviation of the performance metric values of HFCM obtained based on different expert contours.

	Expert 1	Expert 2	Expert 3
Sensitivity (%)	94.87 ± 3.95	93.61 ± 5.30	94.84 ± 4.39
Specificity (%)	97.43 ± 2.55	96.50 ± 3.38	96.23 ± 3.69
Jaccard (%)	84.06 ± 10.96	80.68 ± 10.28	81.27 ± 12.04
Dice (%)	90.87 ± 8.12	88.89 ± 7.62	89.11 ± 8.84
ASSD (mm)	0.09 ± 0.27	0.11 ± 0.26	0.13 ± 0.30
RMSD (mm)	0.06 ± 0.07	0.07 ± 0.07	0.07 ± 0.07
MSSD (mm)	1.69 ± 1.69	2.21 ± 1.89	2.34 ± 2.24

TABLE IV. Mean and standard deviation of the performance metric values of FCM obtained based on different expert contours.

	Expert 1	Expert 2	Expert 3
Sensitivity (%)	94.39 ± 5.52	93.49 ± 5.49	94.84 ± 4.80
Specificity (%)	96.98 ± 2.99	96.20 ± 3.35	95.94 ± 3.84
Jaccard (%)	82.05 ± 11.20	79.52 ± 10.46	80.28 ± 12.35
Dice (%)	89.65 ± 8.31	88.16 ± 7.81	88.47 ± 9.09
ASSD (mm)	0.10 ± 0.28	0.11 ± 0.26	0.13 ± 0.30
RMSD (mm)	0.06 ± 0.07	0.08 ± 0.07	0.08 ± 0.07
MSSD (mm)	1.79 ± 1.68	2.30 ± 1.88	2.42 ± 2.25

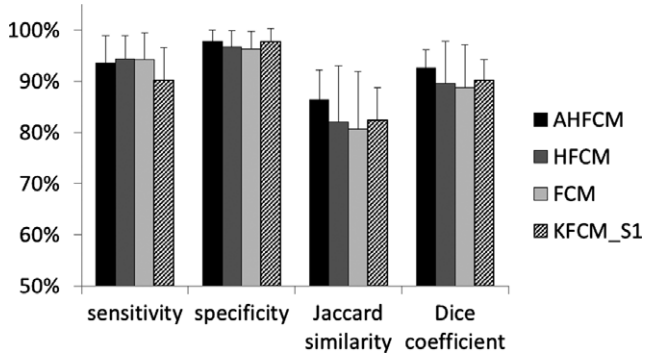

FIG. 7. A comparison of (a) sensitivity, (b) specificity, (c) Jaccard similarity, and (d) Dice coefficient in segmenting the tumor region based on the metric values extracted by three experts.

TABLE V. *P*-values of each evaluation metric from the pairwise Student's *t*-tests by comparing the algorithms.

	AHFCM vs. KFCM_S1	AHFCM vs. HFCM	AHFCM vs. FCM
Sensitivity	0.0221[a]	0.2851	0.4728
Specificity	0.9940	0.0054[a]	0.0057[a]
Jaccard similarity	$< 10^{-3}$ [a]	0.0184[a]	0.0032[a]
Dice coefficient	$< 10^{-3}$ [a]	0.0371[a]	0.0101[a]
ASSD	0.0461	0.1374	0.1050
RMSD	0.1683	0.0452[a]	0.0177[a]
MSSD	0.1142	0.0399[a]	0.0198[a]

[a]A significant difference between the two methods.

breast tumor lesion in US images. The pixel difference was measured by the Hausdorff distance, which includes the neighbor information adaptively changed by comparing the regional mutual information. Compared with the HFCM method for MR images segmentation, which has a fixed region size of 3 × 3 pixels for distance measurement, the inclusion of the adaptive region selection scheme improved the robustness to noise and enhanced the capability to delineate blurred boundaries. These features enable the AHFCM to segment US images. Results showed the proposed algorithm has better performances in segmenting breast tumor lesions in comparison with the FCM with spatial constraints, non-adaptive HFCM, and standard FCM methods.

When segmenting the malignant breast tumors, we observed larger inter-observer variations of the manual segmentation from the experts. This is probably due to the morphological differences between the benign and malignant tumor shapes. The benign tumors have relatively smooth boundaries while the malignant ones have largely unstructured boundaries.[33,34]

Although we observed the overall evaluation metric values of AHFCM were higher than the other methods compared, we observed a lower mean sensitivity than HFCM and FCM. This is because the other two methods tend to segment a region with more pixels rather than a more accurate one. A lower distance based evaluation metrics of AHFCM method demonstrates that the method is more suitable for spatial tracking such as US-image-guided biopsy. Although AHFCM showed to be statistically better than HFCM and FCM in terms of distance metrics, we did not observe a significant better performance than KFCM_S1.

Huang et al. (2012) used a novel graph-based method for segmenting breast tumors. By using graph templates and a predictive function, the algorithm determines the neighboring region information to be merged or not. It was shown that the graph-based segmentation has a better performance than FCM with an average sensitivity value larger than 87% for both benign and malignant tumors. In the current study, we, however, demonstrated that the AHFCM method has a relatively higher sensitivity, probably because the method utilizes larger neighboring information for local pixels. Other US image segmentation techniques applied to breast tumor such as level set[15] and watershed[12,35] were also demonstrated to be effective, but the neighboring information was not fully utilized.

Studies have shown that the inclusion of neighboring information is an effective way to improve the FCM segmentation results.[36–39] Wang and Bu (2010) used a local information map function to modulate the local information and a 5 × 5 fixed window was used to include the neighbor information. Kang et al. (2009), Chen and Zhang (2004) used a 3 × 3 window to incorporate the local information. In this study, we used an adaptive scheme to select the neighbor region. Besides, the Hausdorff distance measures the similarity between the neighbors, which incorporates additional information in distinguishing pixels. Actually, the definition measuring the similarity between the two sets was used to

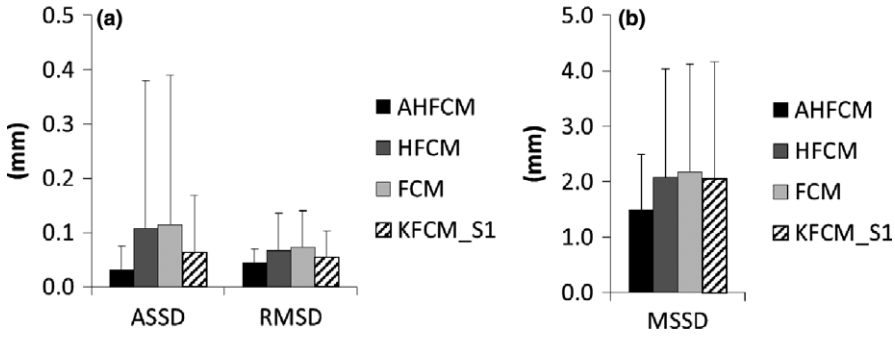

FIG. 8. A comparison of (a) ASSD, RMSD, and (b) MSSD in segmenting the tumor region based on the metric values extracted by three experts.

evaluate segmentation results.[40,41] This improved standard Euclid distance based segmentation,[42] which may also be potentially useful for segmenting images from other modalities.[43–45]

Regarding the FCM based segmentations of the breast tumors, most studies were aimed for MR images, for example, FCM based adaptive k-means cluster to segment breast tissue MR images.[46] With respect to US imaging of breast tumors, Xu and Nishimura (2009) proposed a structure tensor-based method. In their study, the segmentation was carried out in the feature domains of an image where the structure tensor of an image was calculated. The distance between tensors was measured by the Frobenius difference. A larger tolerance to noise was shown than standard FCM. Although part of the pixel neighbor information was integrated into the membership function by a median filter, the algorithm could not select the optimal neighbor region for updating the function. With incorporated adaptive selection of the neighbor information, we significantly improve the FCM in many metrics using a larger sample pool of the breast tumor US images.

5. CONCLUSION

We have developed an adaptive FCM method based on Hausdorff distance definition for segmenting US images of breast cancers through adaptive selection of neighbor region of each pixel for distance measurement and centroid updating. Using clinical US image datasets of breast tumors, we further demonstrated that the proposed method exhibits better performance than the standard FCM and the algorithm without adaptive region selection in terms of region and distance metrics. This suggests that the current method is potentially useful for breast tumor CAD and other US-guided procedures.

ACKNOWLEDGMENTS

Funding is provided by grant 61503267 (YF) from National Natural Science Foundation, grant BK20140356 (YF) from Jiangsu Province, grant 16KJB460018 from Natural Science Research Grant of Higher Education of Jiangsu Province, grant K511701515 (YF) from Scientific Research Foundation for the Returned Overseas Chinese Scholars, State Education Ministry, grant 2016M591905 (YF) from China Postdoctoral Science Foundation, and grant 1601226C (YF) from Jiangsu Planned Projects for Postdoctoral Research Funds. Support from Priority Academic Program Development of Jiangsu Higher Education Institutions (PAPD) is also acknowledged.

CONFLICT OF INTEREST

None.

APPENDIX

The sensitivity C_{sen}, specificity C_{spc}, Jaccard similarity metric C_{jac}, and Dice coefficient C_{dic} are defined as

$$c_{sen} = \frac{|A \cap B|}{|B|}, C_{spc} = \frac{|\overline{A \cup B}|}{|\overline{B}|}, C_{jac} = \frac{|A \cap B|}{|A \cup B|},$$
$$C_{dic} = \frac{2|A \cap B|}{|A| + |B|},$$

where $A = \{p_i | p_i \in A\}$ represents the segmented region, $B = \{p_j | p_j \in B\}$ is the ground truth, and |*| is the size of the non-zero binary set. The average symmetric surface distance (ASSD)[47] is defined as

$$ASSD = \frac{1}{|A| + |B|}\left(\sum_i \inf_{p_j \in B} |p_j - p_i| + \sum_j \inf_{p_i \in A} |p_i - p_j|\right).$$

The root mean square symmetric surface distance (RMSD)[47] is defined as

$$RMSD = \sqrt{\frac{1}{|A| + |B|}\left(\sum_i \inf_{p_j \in B} |p_j - p_i| + \sum_j \inf_{p_i \in A} |p_i - p_j|\right)}.$$

The maximum symmetric surface distance (MSSD) is defined as the same as the Hausdorff distance.

[a]Author to whom correspondence should be addressed. Electronic mail: fengyuan@suda.edu.cn; Telephone: +86 18625085336.

REFERENCES

1. Jemal A, Bray F, Center MM, Ferlay J, Ward E, Forman D. Global cancer statistics. *CA Cancer J Clin*. 2011;61:69–90.

2. Anderson BO, Bevers TB, Carlson RW. CLinical breast examination and breast cancer screening guideline. *JAMA*. 2016;315:1403–1404.
3. Cheng HD, Shan J, Ju W, Guo Y, Zhang L. Automated breast cancer detection and classification using ultrasound images: a survey. *Pattern Recogn*. 2010;43:299–317.
4. Hooley RJ, Greenberg KL, Stackhouse RM, Geisel JL, Butler RS, Philpotts LE. Screening US in patients with mammographically dense breasts: initial experience with Connecticut Public Act 09-41. *Radiology*. 2012;265:59–69.
5. Berg WA, Blume JD, Cormack JB, et al. Combined screening with ultrasound and mammography vs mammography alone in women at elevated risk of breast cancer. *JAMA*. 2008;299:2151–2163.
6. Berg WA, Zhang Z, Lehrer D, et al. Detection of breast cancer with addition of annual screening ultrasound or a single screening mri to mammography in women with elevated breast cancer risk. *JAMA*. 2012;307:1394–1404.
7. Shan J, Alam SK, Garra B, Zhang Y, Ahmed T. Computer-aided diagnosis for breast ultrasound using computerized BI-RADS features and machine learning methods. *Ultrasound Med Biol*. 2016;42:980–988.
8. Cai L, Wang X, Wang Y, Guo Y, Yu J, Wang Y. Robust phase-based texture descriptor for classification of breast ultrasound images. *Biomed Eng Online*. 2015;14:1–21.
9. Kuang Y, Hilgers A, Sadiq M, Cochran S, Corner G, Huang Z. Modelling and characterisation of a ultrasound-actuated needle for improved visibility in ultrasound-guided regional anaesthesia and tissue biopsy. *Ultrasonics*. 2016;69:38–46.
10. Rueda S, Fathima S, Knight CL, et al. Evaluation and comparison of current fetal ultrasound image segmentation methods for biometric measurements: a grand challenge. *IEEE T Med Imaging*. 2014;33:797–813.
11. Noble JA, Boukerroui D. Ultrasound image segmentation: a survey. *IEEE T Med Imaging*. 2006;25:987–1010.
12. Gu P, Lee W-M, Roubidoux MA, Yuan J, Wang X, Carson PL. Automated 3D ultrasound image segmentation to aid breast cancer image interpretation. *Ultrasonics*. 2016;65:51–58.
13. Huang QH, Yang FB, Liu LZ, Li XL. Automatic segmentation of breast lesions for interaction in ultrasonic computer-aided diagnosis. *Inf Sci*. 2015;314:293–310.
14. Huang Q-H, Lee S-Y, Liu L-Z, Lu M-H, Jin L-W, Li A-H. A robust graph-based segmentation method for breast tumors in ultrasound images. *Ultrasonics*. 2012;52:266–275.
15. Guo YH, Sengur A, Tian JW. A novel breast ultrasound image segmentation algorithm based on neutrosophic similarity score and level set. *Comput Meth Programs Biomed*. 2016;123:43–53.
16. Guo Y, Sengur A. NCM: Neutrosophic c-means clustering algorithm. *Pattern Recogn*. 2015;48:2710–2724.
17. Bezdek JC, Hall LO, Clarke LP. Review of MR image segmentation techniques using pattern-recognition. *Med Phys*. 1993;20:1033–1048.
18. Pham DL, Xu CY, Prince JL. Current methods in medical image segmentation. *Annu Rev Biomed Eng*. 2000;2:315–317.
19. B. Z. K, D. W. B. R. S. Presented at the information technology: new generations; 2009. ITNG '09. Sixth International Conference on 2009 (unpublished).
20. Xu Y, Nishimura T. Segmentation of breast lesions in ultrasound images using spatial fuzzy clustering and structure tensors. *Int J Comput Elect Autom Control Inform Eng*. 2009;3:1355–1359.
21. Adhikarla V, Jeraj R. An imaging-based computational model for simulating angiogenesis and tumour oxygenation dynamics. *Phys Med Biol*. 2016;61:3885–3902.
22. Feng Y, Kawrakow I, Olsen J, et al. A comparative study of automatic image segmentation algorithms for target tracking in MR-IGRT. *J Appl Clin Med Phys*. 2016;17:441–460.
23. Khalilia MA, Bezdek J, Popescu M, Keller JM. Improvements to the relational fuzzy c-means clustering algorithm. *Pattern Recogn*. 2014; 47:3920–3930.
24. Pham DL. Spatial models for fuzzy clustering. *Comput Vis Image Und*. 2001;84:285–297.
25. Krishnapuram R, Keller JM. A possibilistic approach to clustering. *IEEE Trans Fuzzy Syst*. 1993;1:98–110.
26. Pal NR, Pal K, Keller JM, Bezdek JC. A possibilistic fuzzy c-means clustering algorithm. *IEEE Trans Fuzzy Syst*. 2005;13:517–530.
27. Hathaway RJ, Bezdek JC. Clustering incomplete relational data using the non-Euclidean relational fuzzy c-means algorithm. *Pattern Recogn Lett*. 2002;23:151–160.
28. Zhao X, Li Y, Zhao Q. Mahalanobis distance based on fuzzy clustering algorithm for image segmentation. *Digit Signal Process*. 2015;43:8–16.
29. Feng Y, Guo H, Zhang H, et al. A modified fuzzy c-means method for segmenting MR images using non-local information. *Technol Health Care*. 2016;24:S785–S793.
30. Chen S, Zhang D. Robust image segmentation using FCM with spatial constraints based on new kernel-induced distance measure. *IEEE Tran Syst Man Cybern B Cybern*. 2004;34:1907–1916.
31. Zhang D-Q, Chen S-C. A novel kernelized fuzzy C-means algorithm with application in medical image segmentation. *Artif Intell Med*. 2004;32:37–50.
32. Filippi M, Horsfield MA, Rovaris M, et al. Intraobserver and interobserver variability in schemes for estimating volume of brain lesions on MR images in multiple sclerosis. *Am J Neuroradiol*. 1998;19:239–244.
33. Stavros AT, Thickman D, Rapp CL, Dennis MA, Parker SH, Sisney GA. Solid breast nodules: use of sonography to distinguish between benign and malignant lesions. *Radiology*. 1995;196:115–116.
34. Gokhale S. Ultrasound characterization of breast masses. *Indian J Radiol Imaging*. 2009;19:242–247.
35. Huang Y-L, Chen D-R. Watershed segmentation for breast tumor in 2-D sonography. *Ultrasound Med Biol*. 2004;30:625–632.
36. Chuang K-S, Tzeng H-L, Chen S, Wu J, Chen T-J. Fuzzy c-means clustering with spatial information for image segmentation. *Comput Med Imaging Graph*. 2006;30:9–15.
37. Ahmed MN, Yamany SM, Mohamed N, Farag AA, Moriarty T. A modified fuzzy C-means algorithm for bias field estimation and segmentation of MRI data. *IEEE Trans Med Imaging*. 2002;21:193–199.
38. Wang X-Y, Bu J. A fast and robust image segmentation using FCM with spatial information. *Digit Signal Process*. 2010;20:1173–1182.
39. Cai W, Chen S, Zhang D. Fast and robust fuzzy c-means clustering algorithms incorporating local information for image segmentation. *Pattern Recogn*. 2007;40:825–838.
40. Noor NM, Than JCM, Rijal OM. Performance evaluation of lung segmentation. In: Lai WK, Octorina Dewi ED, eds. *Medical Imaging Technology: Reviews and Computational Applications*. Singapore: Springer; 2015: 111–127.
41. Noel CE, Zhu F, Lee AY, Yanle H, Parikh PJ. Segmentation precision of abdominal anatomy for MRI-based radiotherapy. *Med Dosim*. 2014; 39:212–217.
42. Tomasi G, Shepherd T, Turkheimer F, Visvikis D, Aboagye E. Comparative assessment of segmentation algorithms for tumor delineation on a test-retest [(11)C]choline dataset. *Med Phys*. 2012;39:7571–7579.
43. Wilde EA, Bouix S, Tate DF, et al. Advanced neuroimaging applied to veterans and service personnel with traumatic brain injury: state of the art and potential benefits. *Brain Imaging Behav*. 2015;9:367–402.
44. Tsien C, Cao Y, Chenevert T. Clinical applications for diffusion magnetic resonance imaging in radiotherapy. *Semin Radiat Oncol*. 2014; 24:218–226.
45. Li H, Chen HC, Dolly S, et al. An integrated model-driven method for in-treatment upper airway motion tracking using cine MRI in head and neck radiation therapy. *Med Phys*. 2016;43:4700.
46. Moftah HM, Azar AT, Al-Shammari ET, Ghali NI, Hassanien AE, Shoman M. Adaptive k-means clustering algorithm for MR breast image segmentation. *Neural Comput Appl*. 2014;24:1917–1928.
47. Haidekker MA. Medical imaging technology. *Radiology*. 1995;196:123–134.